

## Berezinskii-Kosterlitz-Thouless Transition in Two-Dimensional Dipole Systems

A. Filinov,<sup>1,2</sup> N. V. Prokof'ev,<sup>3,4</sup> and M. Bonitz<sup>1</sup>

<sup>1</sup>*Institut für Theoretische Physik und Astrophysik, Christian-Albrechts-Universität, Leibnizstrasse 15, D-24098 Kiel, Germany*

<sup>2</sup>*Institute of Spectroscopy of the Russian Academy of Sciences, Troitsk, Russia*

<sup>3</sup>*Department of Physics, University of Massachusetts, Amherst, Massachusetts 01003, USA*

<sup>4</sup>*Russian Research Center, Kurchatov Institute, 123182 Moscow, Russia*

(Received 21 April 2010; revised manuscript received 14 June 2010; published 9 August 2010)

The superfluid to normal fluid transition of dipolar bosons in two dimensions is studied in a broad density range by using path integral Monte Carlo simulations and summarized in the phase diagram. While at low densities we find good agreement with the universal results depending only on the scattering length  $a_s$ , at moderate and high densities the transition temperature is strongly affected by interactions and the excitation spectrum of quasiparticles. The results are expected to be of relevance to dipolar atomic and molecular systems and indirect excitons in quantum wells.

DOI: 10.1103/PhysRevLett.105.070401

PACS numbers: 05.30.Jp, 03.75.Hh, 67.85.-d

Dipolar bosonic systems are of increasing interest for various recent experiments studying the onset of superfluidity in nonideal Bose systems and its connection with correlation and quantum degeneracy effects. Examples include dipolar gases, as in recent studies of  $^{52}\text{Cr}$  atoms [1], bosonic molecules, e.g., SrO, RbCs, LiCs, and  $^{40}\text{K}^{87}\text{Rb}$  [2], as well as indirect excitons in semiconductor quantum wells [3,4]. A number of theoretical and computational studies have addressed the properties of two-dimensional (2D) repulsive dipolar bosons at zero and low temperatures [5–7]. They include the ground-state energy and the structural and coherence properties, such as the one-body density matrix and the condensate fraction. Quantum Monte Carlo studies at  $T = 0$  have covered the whole range of coupling strengths up to the crystallization transition. However, the finite-temperature properties, in particular, the superfluid transition temperature  $T_c$ , remain unexplored.

Previous numerical investigations for 2D homogeneous Bose gases [8,9] have shown that in the dilute (weak coupling) regime  $na_s^2 \lesssim 10^{-2}$ , where  $n$  is the density and  $a_s$  the  $s$ -wave scattering length, the exact shape of the interaction potential is irrelevant for  $T_c$  which is a function of  $na_s^2$  only [10]:

$$T_c(n) = \frac{2\pi\hbar^2 n}{mk_B} \frac{1}{\ln(\nu/4\pi) + \ln \ln(1/na_s^2)}, \quad (1)$$

where the numerical coefficient is  $\nu = 380(3)$  [11]. However, for moderate and high densities where correlation effects are important, no analytical expression is available for  $T_c$ , calling for investigations by direct numerical simulations which is the main goal of the present paper. By performing first-principles path integral Monte Carlo (PIMC) simulations, we demonstrate that, with increasing interaction strength, the superfluid phase is first stabilized ( $T_c$  increases) and then destabilized and vanishes when the system forms a dipolar solid. This results in a nonmono-

tonic behavior of  $T_c$ . We also discuss whether and how this behavior is related to the excitation spectrum.

*Model and parameters.*—We focus on a pure *dipole model* relevant, e.g., for various bosonic atoms or molecules and indirect excitons at low densities where the dipole moment is a free parameter which can be externally controlled, e.g., via an electric field [4,12]. The 2D dipole system is described by the Hamiltonian

$$\hat{H} = - \sum_{i=1}^N \frac{\hbar^2 \nabla_i^2}{2m} + \frac{1}{2} \sum_{i \neq j} \frac{p^2}{\epsilon_b |\mathbf{r}_i - \mathbf{r}_j|^3}, \quad (2)$$

which is brought to a dimensionless form by using the units  $a = 1/\sqrt{n}$  and  $E_0 = \hbar^2/ma^2$ . The system properties are defined by the dipole coupling  $D = p^2/\epsilon_b a^3 E_0$  and the temperature  $T = k_B T/E_0$ . The thermodynamic equilibrium states of system (2) were sampled by PIMC simulations with the worm algorithm [13]. For each parameter set  $(T, D)$  about  $10^7$  MC samples have been used. The number of time slices has been varied as  $M \sim 1/T$ , with  $M = 200$  for the lowest temperature  $T = 0.5$ . No Ewald summation was used since it has practically no influence on the finite-size scaling of the superfluid density. We studied the system (2) from weak to strong coupling,  $D = 0.01, \dots, 20$ . In agreement with Refs. [5–7] we observe formation of a crystalline phase at  $D \simeq 18$ .

*Superfluid transition and phase diagram.*—In 2D the superfluid-normal phase transition occurs at a finite temperature  $T_c$  and follows the Berezinskii-Kosterlitz-Thouless scenario induced by interaction effects [14]. To obtain a reliable result for  $T_c$  in the thermodynamic limit  $T_c(\infty)$  from simulations of a finite system of size  $L = \sqrt{N}$ , we apply a finite-size scaling analysis to  $T_c(L)$ . We assume the essential singularity [15] of the correlation length  $\xi(T) \sim e^{at^{-1/2}}$ ,  $t = (T/T_c - 1)|_{T \rightarrow T_c}$ , with  $a$  being a non-universal temperature-density-dependent scaling factor. Near  $T_c$  the role of  $\xi$  is taken over by  $L$ , leading to  $[b$  is

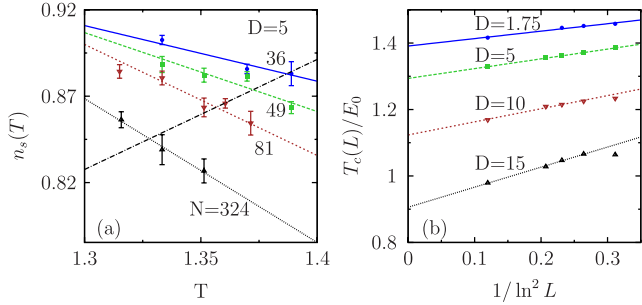


FIG. 1 (color online). (a) Superfluid fraction  $n_s(T)$  for  $D = 5$  and different system sizes  $N = 36, 49, 81,$  and  $324$ . Crossing with the dash-dotted line  $n_s(T_c) = 2mk_B T_c / \pi \hbar^2$  gives the critical temperature  $T_c(L = \sqrt{N})$ . (b) System size scaling of  $T_c(L)$  for several coupling strengths  $D$ .

a constant; cf. Fig. 1(b)]

$$T_c(L) = T_c(\infty) + \frac{b}{\ln^2(L)}, \quad n_s(T_c, L) = \frac{2mk_B}{\pi \hbar^2} T_c, \quad (3)$$

where  $T_c(L)$  is determined by the scenario of the universal jump of the superfluid fraction (second equation) [16]. Here, the superfluid density  $n_s$  is obtained via the *winding number* estimator [17]  $n_s(T, L) = mk_B T \langle \mathbf{W}^2 \rangle (T, L) / 2\hbar^2$ , which is directly evaluated by PIMC simulations.

In Fig. 1, we show the temperature dependence and the finite-size scaling of  $n_s(T, L)$  and  $T_c(L)$ . We observe that  $T_c(L)$  shifts systematically with  $L$  to lower values [Fig. 1(a)]. The extrapolation to the thermodynamic limit  $T_c(\infty)$ , fitting the simulation data by Eq. (3), is reported in Fig. 1(b). For strong coupling ( $D \geq 10$ ) the finite-size corrections to  $T_c$  become important; therefore, we excluded from the fit the smallest system ( $N = 36$ ).

Using the extrapolated data  $T_c(\infty, D)$ , we construct the phase diagram; cf. Fig. 2 and Table I. At small coupling  $D \leq 0.01$ , our results are well reproduced by the asymptotic expression (1); i.e., here, details of the interaction potential are not important. However, the validity range of Eq. (1) is limited to very low densities  $na_s^2 \lesssim 10^{-3}$  [computing the scattering length from the solution of the Schrödinger equation for 2D dipoles gives the relation  $na_s^2 \approx 10.05D^2$ ]. This density is an order of magnitude smaller than for a 2D gas of hard disks [9], indicating that the long-range character of the dipole interaction causes substantially earlier deviations from the dilute gas limit.

Now we analyze the change of the superfluid transition temperature  $T_c$  with coupling (Fig. 2). For small  $D$ ,  $T_c$  monotonically increases and reaches a maximum around  $1 < D < 2$ , whereas, for larger couplings,  $T_c$  monotonically decreases again until the system freezes into a non-superfluid dipole crystal. This is preceded by a narrow hysteresis region ( $15 < D < 18$ ), shown by the vertical dashed lines, where a bubble-type structure is expected [18], which, however, is beyond the scope of the present Letter.

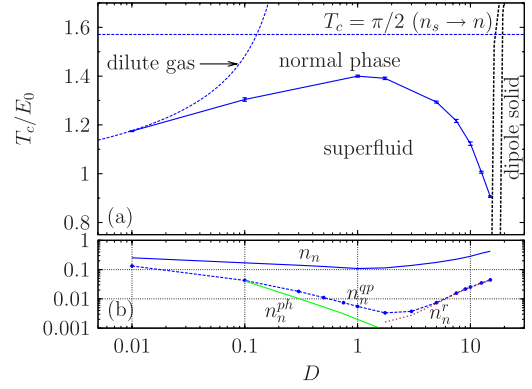


FIG. 2 (color online). (a) Phase diagram in the  $T$ - $D$  plane. The system is superfluid below the solid (blue) line. The two vertical dashed lines bound the gas-solid hysteresis region to the right of which the system is in a dipole crystal phase [5–7,27]. The horizontal dashed line is the upper bound for  $T_c$  obtained by replacing  $n_s \rightarrow n$ . The dotted line denotes the estimate for  $T_c$  according to Eq. (1). (b)  $D$  dependence of the normal density  $n_n$  (PIMC result), the quasiparticle contribution  $n_n^{\text{QP}}$  [Eq. (6)], and the phonon-roton contribution [Eqs. (7) and (8), respectively] for  $T = T_c$ . The difference  $n_n^m = n_n - n_n^{\text{QP}}$  is given in Table I.

Since in 2D the critical temperature and normal density are linearly related to each other,  $T_c \propto n_s(T_c) = n - n_n(T_c)$ , the maximum of  $T_c$  (at fixed total density) corresponds to the minimum of  $n_n$  around  $D \sim 1.75$ . It is thus interesting to investigate to what degree the normal density is described by a quasiparticle (QP) picture and whether  $n_n$  is dominated by the phonon and roton quasiparticle excitations similarly to the bulk  $^4\text{He}$  superfluid. For the Berezinskii-Kosterlitz-Thouless transition one expects that vortices play an important role, especially for large vortex fugacity. Below, we will show that in the present system, indeed, the QP contribution  $n_n^{\text{QP}}(T_c, D)$  to the full normal density is low.

*Excitation spectrum.*—The excitation spectrum  $\omega(q)$  has an upper bound given by the Feynman relation [19]

TABLE I. Coupling parameter dependence of the superfluid transition temperature  $T_c$ , the superfluid fraction  $\gamma_s(T_c) = 2mT_c / \pi \hbar^2 n$ , the sound speed  $c$  [in units of the dipole frequency ( $\omega_D \bar{a}$ ),  $\omega_D^2 = 2\pi p^2 n / (m \bar{a}^3)$ , and  $\bar{a} = (\pi n)^{-1/2}$ ], the roton gap  $\Delta$ , and the missing normal density  $n_n^m(T_c)$ .

| $D$  | $T_c [E_0]$ | $\gamma_s(T_c)$ | $c$  | $\Delta [E_0]$ | $n_n^m(T_c)$ |
|------|-------------|-----------------|------|----------------|--------------|
| 0.01 | 1.174(2)    | 0.75            | 3.60 | ...            | 0.12         |
| 0.1  | 1.304(7)    | 0.83            | 2.23 | ...            | 0.13         |
| 1    | 1.400(4)    | 0.89            | 1.59 | ...            | 0.10         |
| 1.75 | 1.391(5)    | 0.88            | 1.48 | 13.02          | 0.11         |
| 3    | 1.353(5)    | 0.86            | 1.41 | 11.73          | 0.13         |
| 5    | 1.294(4)    | 0.82            | 1.36 | 10.00          | 0.17         |
| 7.5  | 1.216(6)    | 0.77            | 1.31 | 8.35           | 0.21         |
| 10   | 1.123(7)    | 0.71            | 1.30 | 7.12           | 0.26         |
| 12.5 | 1.006(4)    | 0.64            | 1.28 | 6.06           | 0.32         |
| 15   | 0.906(3)    | 0.58            | 1.28 | 5.27           | 0.38         |

generalized to finite temperatures:

$$\omega(q) \leq \omega_F(q), \quad \omega_F(q) \tanh\left[\frac{\hbar\omega_F(q)}{2T}\right] = \frac{\hbar q^2}{2mS(q, T)}, \quad (4)$$

where  $S(q, T)$  is the static structure factor. The latter was computed below and above  $T_c$ :  $0.5 \leq T \leq 3.3$ ; cf. Fig. 3(a). As  $D$  approaches the crystallization point, a sharp peak develops near the wave number  $q_0$  corresponding to the mean interparticle distance  $q_0 a = 2\pi$ . While  $S(q, T)$  shows some  $T$  dependence for  $qa < 3$ ,  $\omega_F(q, T)$  stays almost unchanged in a broad temperature interval  $T \lesssim 3.3$  and is close to the ground-state result [7,20]. Therefore, the spectra shown in Fig. 4 for  $T = 0.5$  are representative for the low-temperature behavior.

In the long wavelength limit  $qa \rightarrow 0$ ,  $\omega_F$  yields a linear dispersion:  $\omega_F(q) = cq$ ; cf. Fig. 4(a), which is in agreement with the result for classical 2D dipoles [21,22]. Our results for the sound speed,  $c(T) = \omega_F(q, T)/q|_{q \rightarrow 0}$ , extracted from the data for  $N = 324$  particles are summarized in Table I and agree within 4% with the ground-state values of Ref. [7].

A significant improvement of the spectrum is achieved by using a sum-rule approach [23,24] by combining the PIMC results for  $S(q, T)$  and the static density response function  $\chi(q, T)$ . This yields a rigorous upper bound

$$\hbar\omega(q) \leq \hbar\omega_\chi(q, T) = 2nS(q, T)/\chi(q, T),$$

$$\chi(q) = -\int_0^\beta F(q, \tau) d\tau, \quad F(q, \tau) = \frac{1}{N} \langle \hat{\rho}_q(\tau) \hat{\rho}_q(0) \rangle, \quad (5)$$

where  $\chi(q)$  is obtained from the imaginary-time density-density correlation function  $F(q, \tau)$  directly evaluated in our PIMC simulations. With the increase of  $D$ ,  $\chi(q)$  sharpens and its peak shifts continuously towards  $q_0$ ; cf. Fig. 3(b).

In Fig. 4, we show  $\omega_\chi$  [Eq. (5)] together with the Feynman spectrum and the correlated basis functions (CBF) result [25] at four dipole couplings. All three approximations show the same general trend which resem-

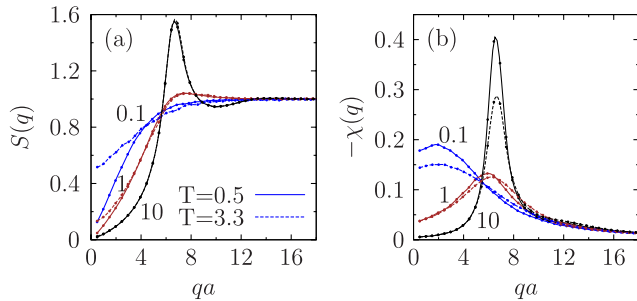


FIG. 3 (color online). (a) Static structure factor and (b) density response function at  $T = 0.5$  (solid lines) and  $T = 3.3$  (dashed lines) for three couplings  $D = 0.1, 1$ , and  $10$  (numbers in the figure).

bles superfluid helium: With increasing coupling the spectrum develops a roton minimum at finite  $q \approx q_0$  which becomes deeper with increasing  $D$ . While for  $qa \leq 1.5$  (sound range) all approaches are in quantitative agreement, for  $qa > 2$  the Feynman approximation becomes inaccurate. Its error increases with  $D$  and exceeds 100% at the crystallization point for  $\omega(q_0)$ . The PIMC result  $\omega_\chi(q)$  agrees surprisingly well with  $\omega_{\text{CBF}}(q)$ . Our simulations predict a deeper minimum  $\omega(q_0)$  and are expected to be more accurate here. Furthermore, for  $q \gtrsim 7.5$ , the upper bound  $\omega_\chi(q)$  approaches a free-particle spectrum (similar to  $\omega_F$ ), except for  $D \gtrsim 15$ , whereas CBF, at strong coupling ( $D = 15$ ), shows the onset of a plateau. In analogy with superfluid  $^4\text{He}$  a plateau might be expected at twice the roton minimum energy, but it appears that all schemes violate this threshold which calls for further improvement of the theory.

The obtained spectra  $\omega_\chi(p)$  allow us, via a numerical fit, to extract the important parameters ( $c$ ,  $\Delta$ ,  $p_0$ , and  $\mu$ ) of the lowest energy quasiparticles: phonons with the dispersion  $\varepsilon_p^{\text{ph}} = cp$  and rotons  $\varepsilon_p^r = \Delta + (p - p_0)^2/2\mu$ . The roton gap  $\Delta$  (cf. Table I) in the liquid phase is found to decrease exponentially with the dipole coupling:  $\Delta(D)/E_0 = a_1 \exp(-a_2 D - a_3 D^2)$ , with the best fit parameters:  $a_1 = 15.11(5)$ ,  $a_2 = 0.088(2)$ , and  $a_3 = -0.00120(8)$ , whereas at the crystallization point we find  $\Delta(D = 18)/E_0 = 4.57$ .

*QP contribution to the normal density.*—While PIMC simulations yield accurate results to the excitation spectrum, they do not directly provide access to dynamical properties. Therefore, we can only estimate the QP contribution to the normal density by using the Landau formula for noninteracting quasiparticles [26] together with the computed excitation spectrum  $\varepsilon_p = \hbar\omega_\chi(p; D, T)$  (we used  $m = 1$ ):

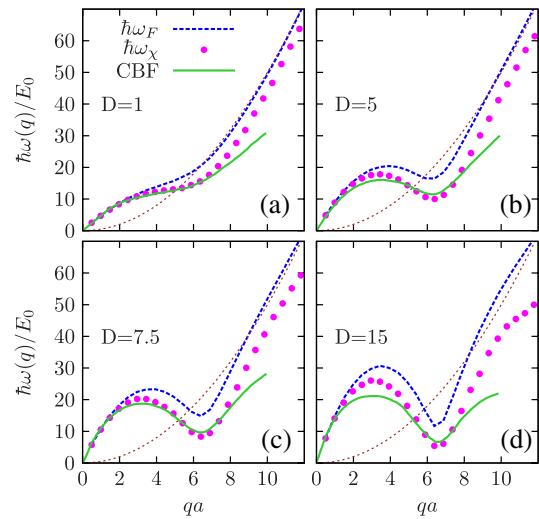


FIG. 4 (color online). Excitation spectrum  $\varepsilon_q = \hbar\omega(q, T)$  for  $T = 0.5$  and different couplings  $D$ . PIMC results  $\omega_F$  [Eq. (4)] and  $\omega_\chi$  [Eq. (5)] are compared with the CBF spectra ( $D = 1, 4, 8$ , and  $16$ ), Ref. [25], and  $(\hbar q)^2/2m$  (short dashed lines).

$$n_n^{\text{QP}}(T) = -\frac{1}{2} \frac{1}{(2\pi\hbar)^2} \int_0^\infty d^2 p p^2 \frac{dn_B}{d\varepsilon_p}, \quad (6)$$

where  $n_B = [e^{\beta\varepsilon_p} - 1]^{-1}$  is the Bose distribution function.

At low temperatures the main contribution to  $n_n^{\text{QP}}$  comes from phonons and rotons [26] with the following result in 2D:

$$n_n^{\text{ph}} = \frac{3\bar{\varepsilon}_{\text{ph}}}{2c^2} = \frac{3\zeta(3)}{2\pi} \frac{(k_B T)^3}{\hbar^2 c^4} = 0.574 \frac{(k_B T)^3}{\hbar^2 c^4}, \quad (7)$$

$$n_n^r \approx \frac{\beta p_0^2}{2} n_r, \quad n_r(T) = \frac{p_0}{2\pi\hbar^2} e^{-\beta\Delta} (2\pi\mu k_B T)^{1/2}. \quad (8)$$

The  $D$  dependence of  $n_n^{\text{ph}}$ ,  $n_n^r$ , and  $n_n^{\text{QP}}$  (6) is shown in Fig. 2(b). At weak coupling  $D \lesssim 1$ , there is no roton minimum in the spectrum [cf. Fig. 4,  $D = 1$ ] and  $n_n^r = 0$ ,  $n_n^{\text{ph}} \approx n_n^{\text{QP}}$ . By increasing  $D$ , the QP contribution  $n_n^{\text{QP}}$  to the normal density monotonically decreases from 53%, at  $D = 0.01$ , to 3% at  $D = 1.75$ –3. This is due to the monotonic decrease of  $n_n^{\text{ph}}$  with  $D$  since, at a fixed temperature, the sound speed increases with coupling,  $c \sim D^{1/2}$ ; cf. Table I. This tendency is reversed with the formation of the roton minimum. For  $D \gtrsim 1.75$  (cf. Fig. 4), the phonon excitations are practically negligible and the rotons dominate due to the larger density of states ( $\sim qdq$ ). The roton density  $n_n^r \approx n_n^{\text{QP}}$  monotonically increases with  $D$  [cf. Fig. 2(b)] due to the reduction of the roton gap; cf. Table I. Near crystallization ( $D = 15$ ) the contribution of quasiparticles to  $n_n$  increases to 10%.

These competing trends of phonons and rotons give rise to a minimum in the sum  $n_n^{\text{ph}}(D) + n_n^r(D)$  at a coupling around  $D = 1.75$  which rather well reproduces the full quasiparticle density  $n_n^{\text{QP}}(D)$ . We notice that the position of this minimum is very close to the maximum of the superfluid transition temperature  $T_c$  which is observed in the range  $D \approx 1$ –1.75. Yet this agreement is not sufficient to explain the nonmonotonic behavior of  $T_c$ , as the picture of noninteracting QP accounts just for a few percent of the normal density which is by itself an unexpected result. The  $D$  dependence of the “missing” normal density  $n_n^m = n_n - n_n^{\text{QP}}$  is listed in Table I. This density can arise from a variety of effects such as interactions of quasiparticles, multiexcitations [25], and vortices. In particular, large scale vortices are key for the Berezinskii-Kosterlitz-Thouless theory.

In conclusion, the finite-temperature phase diagram of a 2D dipole system has been investigated by first-principles PIMC simulations over the entire coupling regime. We found that the superfluid density at  $T_c$  does not exceed 90% and drops to about 58% near the crystallization point. An upper bound for the single-particle spectrum has been computed which significantly improves the result of the Feynman approximation. The superfluid transition temperature shows a nonmonotonic behavior with a maximum observed around  $D = 1.75$  which coincides with the ap-

pearance of a roton minimum in the excitation spectrum. We expect that our predictions are of direct relevance for the experimental search for superfluidity in atomic and molecular dipole systems as well as for indirect excitons or polaritons in semiconductor quantum wells. Our results for  $T_c$  should allow us to determine the optimal parameters in the experiments.

This work is supported by the Deutsche Forschungsgemeinschaft via Grant No. FI 1252/1.

- 
- [1] A. Griesmaier *et al.*, *Phys. Rev. Lett.* **94**, 160401 (2005).
  - [2] For a recent overview, see T. Lahaye *et al.*, *Rep. Prog. Phys.* **72**, 126401 (2009).
  - [3] V. Negoita *et al.*, *Phys. Rev. B* **60**, 2661 (1999); L. Butov *et al.*, *Nature (London)* **417**, 47 (2002); A. Hammack *et al.*, *Phys. Rev. Lett.* **96**, 227402 (2006); V. Timofeev *et al.*, *J. Phys. Condens. Matter* **19**, 295209 (2007).
  - [4] P. Ludwig *et al.*, *Phys. Status Solidi B* **243**, 2363 (2006); A. Filinov *et al.*, *J. Phys. A* **42**, 214016 (2009).
  - [5] C. Mora *et al.*, *Phys. Rev. B* **76**, 064511 (2007).
  - [6] H. Büchler *et al.*, *Phys. Rev. Lett.* **98**, 060404 (2007).
  - [7] G. Astrakharchik *et al.*, *Phys. Rev. Lett.* **98**, 060405 (2007).
  - [8] S. Pilati *et al.*, *Phys. Rev. A* **71**, 023605 (2005); G. Astrakharchik *et al.*, *Phys. Rev. A* **75**, 063630 (2007).
  - [9] S. Pilati, S. Giorgini, and N. Prokof'ev, *Phys. Rev. Lett.* **100**, 140405 (2008).
  - [10] V.N. Popov, *Functional Integrals and Collective Excitations* (Cambridge University Press, Cambridge, England, 1999); D.S. Fisher and P.C. Hohenberg, *Phys. Rev. B* **37**, 4936 (1988).
  - [11] N.V. Prokof'ev *et al.*, *Phys. Rev. Lett.* **87**, 270402 (2001).
  - [12] A. Micheli *et al.*, *Phys. Rev. A* **76**, 043604 (2007).
  - [13] M. Boninsegni, N.V. Prokof'ev, and B.V. Svistunov, *Phys. Rev. E* **74**, 036701 (2006).
  - [14] V.L. Berezinskii, *Sov. Phys. JETP* **32**, 493 (1971); J. Kosterlitz and D. Thouless, *J. Phys. C* **6**, 1181 (1973).
  - [15] J. Kosterlitz, *J. Phys. C* **7**, 1046 (1974).
  - [16] D.R. Nelson and J.M. Kosterlitz, *Phys. Rev. Lett.* **39**, 1201 (1977).
  - [17] D. Ceperley, *Rev. Mod. Phys.* **71**, S438 (1999).
  - [18] B. Spivak and S.A. Kivelson, *Phys. Rev. B* **70**, 155114 (2004).
  - [19] A. Bijl, *Physica (Utrecht)* **7**, 869 (1940); R. Feynman, *Phys. Rev.* **94**, 262 (1954).
  - [20] A similar weak temperature dependence of the excitation spectrum was also observed for liquid helium up to  $T \sim 2T_\lambda$ : E. Svensson *et al.*, *Phys. Rev. B* **21**, 3638 (1980).
  - [21] D.M. Kachintsev and S.E. Ulloa, *Phys. Rev. B* **50**, 8715 (1994).
  - [22] G. Kalman *et al.*, *Phys. Rev. Lett.* **98**, 236801 (2007).
  - [23] S. Stringari, *Phys. Rev. B* **46**, 2974 (1992); J. Boronat *et al.*, *ibid.* **52**, 1236 (1995).
  - [24] S. Moroni, S. Conti, and M.P. Tosi, *Phys. Rev. B* **53**, 9688 (1996).
  - [25] F. Mazzanti *et al.*, *Phys. Rev. Lett.* **102**, 110405 (2009).
  - [26] E.M. Lifshitz and L.M. Pitaevskii, *Statistical Physics* (Pergamon, New York, 1980), Vol. 9.
  - [27] R. Kalia and P. Vashishta, *J. Phys. C* **14**, L643 (1981).